ILASS 2008
Sep. 8-10, 2008, Como Lake, Italy

Paper ID ILASS08-3-3

A STUDY OF VORTEX BREAKDOWN IN SUPERCRITICAL FLUIDS

Loren Crook and Paul E. Sojka

Maurice J. Zucrow Laboratories, School of Mechanical Engineering, Purdue University

ABSTRACT
A numerical and experimental investigation of vortex breakdown (VB) was undertaken to i) design an injector capable of producing VB, and ii) to experimentally observe VB. A 3-dimensional model of an axial-plus-tangential swirl generator was developed based on the CFD package Fluent. The input mass ratio (tangential/total) was varied and the momentum swirl number was calculated to generate a curve of swirl number versus mass ratio. This information was used to drive an experimental investigation of the supercritical injection of carbon dioxide into an environment above the critical point (reduced temperatures of 1.01 to 1.10 and reduced pressures of 1.01 to 1.10). Schlieren imaging was used to visualize the flow field and digital images were taken at each operating condition. Spreading angles were measured for each condition, and the occurence of VB was identified in the high-swirl case.

INTRODUCTION

The occurrence of vortex breakdown (VB) was originally discovered more than 50 years ago [1], and the investigation of its underlying mechanisms has been the subject of numerous experimental, numerical and analytical studies in the intervening years [2-4]. It is found to occur in various applications including aerodynamics, combustion and geophysics.

The main motivation for VB research is due to a single application: flow over swept wings at high angles of attack, as is commonly found in fighter aircraft. In this instance, VB can induce flow asymmetries over the wings and control surfaces, resulting in roll moments and making flight control more difficult. Prediction of VB onset location, size and strength are vital to mitigating its adverse effects.

The description of VB is reasonably well agreed-upon. VB occurs in swirling flows with sufficient swirl strength. The degree of swirl is characterized by a dimensionless swirl number, with three common definitions used in the literature. These include the momentum swirl number [5], the velocity swirl number [6] and the circulation swirl number [7]. In the present work, only the momentum swirl number, S_m, is utilized. According to Beer [5], the onset of VB occurs in the range $0.4 < S_m < 0.6$, with S_m given as

$$S_m = \frac{G_\phi}{G_x r} \tag{1}$$

G_ϕ is the integrated angular momentum, G_x is the integrated axial momentum and r is the swirler radius.

A characteristic of VB is the change to the velocity field. At low swirl, the axial velocity has a Gaussian profile. At high degrees of swirl, strong radial and axial pressure gradients occur in the flow, retarding the velocity on the centreline, and causing a “double-hump” profile. The vortex core swells, a recirculation zone develops, and the vortex breaks down.

Flow visualizations [6,8] reveal that the structure of VB has two general forms: bubble and spiral. In bubble VB, which is nearly axisymmetric, a large, slow recirculation zone is apparent immediately downstream of a stagnation point. Spiral VB does not exhibit a steady stagnation point nor is it axisymmetric, but is clearly an abrupt change in the vortical structure.

VB has been observed in gas turbine fuel injectors [9], and is cited as the source of flow instabilities [10,11]. These results are cause for concern to combustor designers, as fuel flow instabilities may likewise produce combustor oscillations and instability. The use of fuel as a heat-sink in future aircraft fuel systems provides impetus to fully understand the nature of supercritical fuel VB [12].

The present study is concerned with examining VB occurring in a supercritical fuel injector. Supercritical is defined here as the fluid being above both its critical pressure and temperature. For the present results, the injectant (CO_2) is above the critical point before and after injection. Thus, any complicating effects due to heat transfer or volumetric expansion are avoided.

According to the literature, this study is the first to examine VB occurring in a supercritical fluid. As such, some numerical work was undertaken prior to any experimental effort. This allowed for the design of the supercritical VB injector, as well as some prediction of its output swirl numbers, according to the inputs of axial and tangential mass flow.

COMPUTATIONAL MODELLING

VB is extremely sensitive to the amount of swirl in a flow, and this dictates the need to precisely control swirl during

experimental efforts. Previous supercritical studies used either straight bore (S_m=0) [13] or fixed swirl number injectors [14]. These are inadequate for the present study.

The simplest type of injector with variable swirl is the axial-plus-tangential geometry, as described by Beer [15]. In this injector, the level of swirl is controlled by the ratio of tangential mass flow to total mass flow. An increase in mass flow ratio provides a subsequent increase in swirl number. The relation between input mass flow ratio and output momentum swirl number is not linear due to VB, and is difficult to predict analytically.

Therefore, a computational study was undertaken to aid in the development of an injector for use in studying supercritical VB. The goal was to predict the output swirl number for a variety of mass ratios, and validate the model with previous experimental work [15]. The results allow the experimenter confident prediction of swirl number by dictating the input mass flow ratio to the injector. This is easily accomplished in the lab by independently controlling the axial and tangential inputs via separate control valves.

The fully 3-dimensional, turbulent Navier-Stokes equations were solved using the Fluent CFD package. The solution was obtained using the Reynolds-averaged Navier-Stokes equations (RANS), the SIMPLE pressure-velocity algorithm, and the Reynolds Stress Model (RSM) for closure of the turbulence problem. As discussed by Pope [16], the simpler k-ε and k-ω turbulence models are less reliable in situations of strong swirl.

The boundary conditions are an axial mass flow inlet, four tangential mass flow inlets, solid walls for the injector swirl chamber and centerbody, and a pressure outlet. The mass flow inlets have 1-dimensional velocity profiles, and a small, positive gauge pressure. The pressure outlet is set to a gauge pressure of zero. These conditions are in agreement with those seen in the experimental work of Beer [15].

The unstructured computational grid is shown in Figure 1, where red indicates the pressure outlet boundary condition, blue indicates a mass flow inlet, and green indicates a solid wall. It contains 6×10^5 tetrahedral cells.

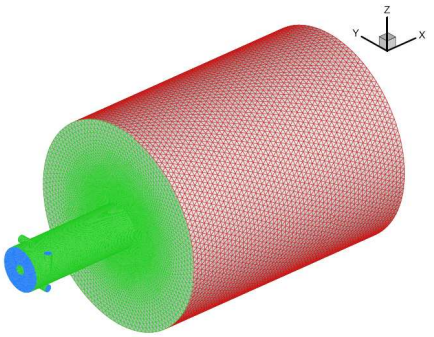

Figure 1. Grid for VB swirl injector computational model.

Four modelled flow fields are shown in Figure 2. The results shown are a single plane of data taken from the 3-dimenasional solution. These vary according to input mass ratio, 0%, 24%, 32% and 69% for Figures 2a, b, c and d, respectively. They represent a broad range of resulting swirl numbers, 0.0, 0.32, 0.66, and 1.78.

The figures show the change in axial velocity profile as the swirl increases. For low-swirl, the jet width increases slightly, and for intermediate (0.66) and high swirl (1.78), the effects of VB are evident as the jet begins to break up and reverse flow regions develop.

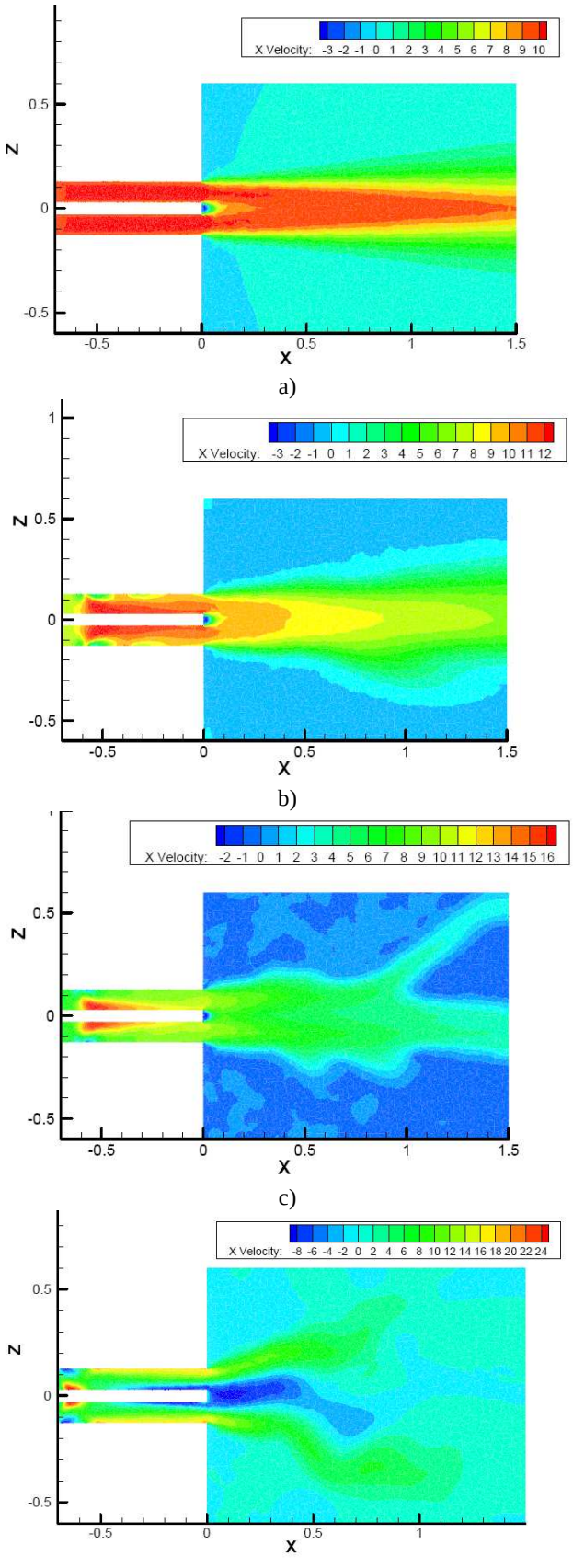

Figure 2. Summary of computation results for mass ratios of a) 0%, b) 24%, c) 32% and d) 60%. All plots indicate x (axial) velocity.

The results of the computational modelling for various output swirl number are shown in Figure 3, which contains two data sets. The first is the measurements of integrated swirl number made by Chigier [15] for their air swirler as a function of mass ratio. The second data set is the results of the computational modelling.

The Chigier [15] swirler includes a solid centerbody in its design, making the injector geometry annular. In their apparatus, this centerbody was to inject additional fuel directly into the swirl-stabilized VB region. This feature was incorporated in the supercritical VB injector, but for a different reason: the boundary-condition at the injector exit is well-defined, and the center body prevents the VB from travelling upstream to the interior, where experimental observation is made difficult due to facility constraints.

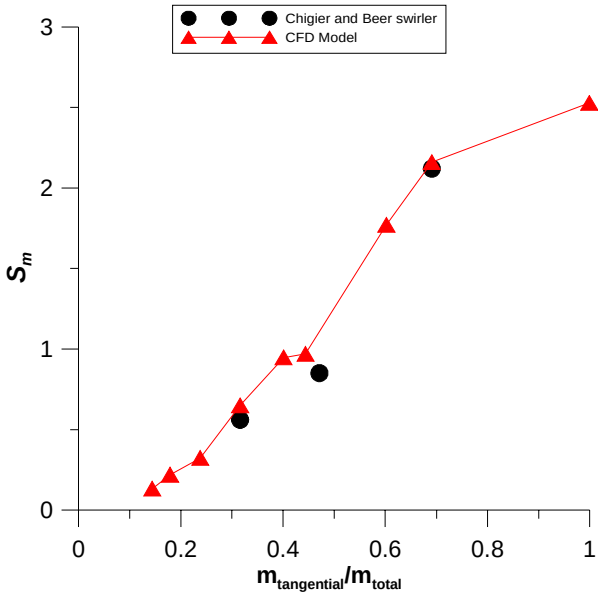

Figure 3. Computational model results. Swirl number as a function of input mass ratio, as compared to the air-swirler of Chigier [15].

Two comments are in order. First, the model consistently over-predicts the swirl number, by 16% for m_{ratio}=31.6% and 2% for m_{ratio}=69.1%. The over-prediction at low mass ratio is due to the fact that the swirl number for the model was calculated at precisely the injector exit, while Chigier [15] was forced to make measurements slightly downstream of this point. The large error (16%) occurs in the VB onset region, which is highly non-linear. Small uncertainties in the actual value of the mass ratio lead to unpredictable differences in S_m in this zone.

Second, the resulting swirl number versus mass ratio curve is highly non-linear over the entire range of ratios examined in this study. However, the low-swirl region (S_m<0.4) is linear, in agreement with the experimental measurements made by Chigier [15].

EXPERIMENTAL APPARATUS

An existing supercritical injection facility at the Maurice J. Zucrow Laboratories at Purdue University was utilized for the experimental portion of the study. The components of the facility are described below.

The single most important item is the VB injector. A section view of it is shown in Figure 4. The items of note are the tangential and axial mass flow inlets, the swirl chamber (where axial and tangential streams mix prior to injection), and the annular injector exit. The centerbody diameter is 1.6 mm, and the annular exit is 7 mm in diameter. The swirl chamber length, from tangential inlets to annular exit, is 18 mm.

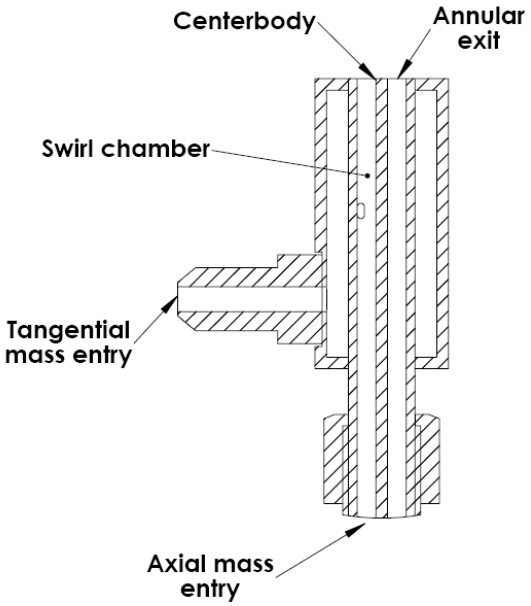

Figure 4. VB injector, axial-plus-tangential swirl design.

The injector was operated inside of a pressure vessel, capable of maintaining an injection environment up to 10.3 MPa and 93° C. Optical access to the vessel interior was obtained via two diametrically-opposed 6.3 cm quartz windows mounted in the vessel walls.

An axisymmetric air co-flow was supplied to the vessel through its top. Honeycomb flow straighteners were mounted upstream and downstream of the injector to establish a nearly one dimensional co-flow.

An accumulator was included in the flow path to damp out oscillations resulting from the CO_2 pressurization process. Experimental data showed mass flowrate oscillations were at most ±5% of the mean.

The source for CO_2 was five 22.7 kg cylinders. The CO_2 temperature was controlled by passing it over electrical immersion heaters, and monitored upstream of the swirl chamber using thermocouples. Separate thermocouples were placed in the tangential and axial mass flows to ensure near-identical temperatures prior to injection. The vessel and CO_2 pressures were monitored using zero-calibrated pressure transducers.

Mass flow rates were measured using Micro Motion coriolis-type flow meters. National Instruments SCXI data hardware and LabVIEW software were utilized for system control and data acquisition.

Special care was taken to ensure that the jets were nearly isothermal and isobaric. This was necessary to restrict changes in the jet refractive index variation to the variation in the CO_2 level. To this end, the axial temperature variation along the jet was measured and observed to be within ±2°C for all schlieren images taken. In addition, the air co-flow temperature (measured just upstream of the injector, in the annulus between the injector body and the test vessel wall) was also kept to within ±2°C of the jet temperature. It was

assumed that because of the turbulent nature of the jet (Reynolds numbers ~10^4), if axial temperature gradients were negligible then radial gradients were also negligible. Finally, pressure variations in the jet, given by the Bernoulli equation, were found to be at most 0.036 MPa.

The schlieren system is a typical Herschellian z-type arrangement, as described by Settles [17]. It uses two identical, oppositely tilted, 108 mm diameter f/6 parabolic telescope mirrors. Tilt angles are kept small (<3 degrees) to reduce astigmatic aberrations. The light source was a 1 kW ellipsoidal theatre lamp. A Phantom camera was used to collect time-resolved high-speed video, which could be separated into individual images, and then time-averaged using a MATLAB routine.

A grid was used to check for barrel- or pincushion-distortion in the schlieren image. Digital photos were taken; neither type of distortion was detected.

Experimental uncertainties in cone angle were calculated using standard techniques [14] and typically found to be ±4.1%. Mass flow rate experimental uncertainties were obtained via water-flow calibration and were found to be ±4.0%. Swirl numbers for each operating condition were interpolated from the mass ratio versus swirl number curve obtained from the computational results. Uncertainties in swirl number were ±1.2%. Uncertainties in density ratio (CO_2/air) due to pressure and temperature measurement uncertainty were ±6.7%.

RESULTS AND DISCUSSION

The sensitivity of the schlieren system to detect light refraction due to refractive index inhomogeneities was calculated to be 48 arcseconds, according to Settles [17]. The measurement range for the schlieren system was calculated to be 907 arcseconds, which corresponds to a maximum refractive index ratio of 1.0022.

The refractive index of single-component fluids can be calculated from the Gladstone-Dale relation

$$\frac{n^2-1}{n^2+2} = k_{GD}\rho \qquad (2)$$

Here n is the refractive index, k_{GD}, is the Gladstone-Dale coefficient and ρ is the fluid density. The calculated refractivity (n-1) of supercritical CO_2 varied according to temperature and pressure. Table 1 is a summary of the refractivity of CO_2 at three test conditions where measurements were made. These are compared with air to illustrate the large refractivity gradient for the test conditions. In fact, during the actual experiments, the solid jet of supercritical CO_2 was visible to the naked eye and was transparent in appearance. This suggests that different optical diagnostics be employed in future studies and perhaps reveal more about the sprays. In particular, laser Doppler anemometry or particle image velocimetry with appropriate seeding could yield detailed velocity field information.

Table 1. Air and CO_2 refractive indices at supercritical test conditions. Calculated from the Gladstone-Dale relation.

Tr	Pr	n_{air}	n_{CO2}
1.001	1.001	0.029	0.122
1.01	1.01	0.029	0.097
1.05	1.05	0.029	0.076
1.10	1.10	0.028	0.067

In schlieren technique, when the measuring range is exceeded regions of the image appear black, indicating that the refractive index gradient was strong enough to refract the collimated light entirely onto the knife-edge. See Figure 5. The lighter region at the jet center is where collimated light passed through without refracting. Thus we know that the background illumination was intense enough for the light to pass through the jet, and except for this center region, the light refracted strongly enough to displace entirely onto the knife-edge.

For the test conditions of Figure 5 (Tr=1.05, Pr=1.05), the refractive index ratio (n_{air}/n_{CO2} = 1.046) dictates a maximum refractive displacement of 18.8×10^3 arcseconds, which greatly exceeds the system maximum (0.95×10^3 arseconds). This is contrasted with the image of subcritical CO_2 injection where n_{air}/n_{CO2} = 1.002, and the maximum refraction angle is 0.79×10^3 arseconds, shown in Figure 6. Here, the system measuring range is nowhere exceeded, and the contrast in the image indicates the concentration changes in the jet from pure CO_2 to pure air.

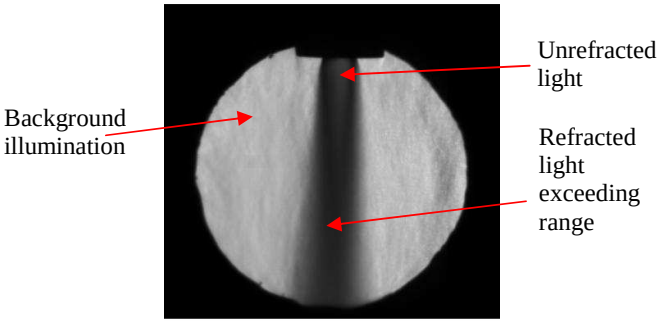

Figure 5. Supercritical injection at Tr=1.05, Pr=1.05, m_{ratio} = 0.0, S_m=0.0.

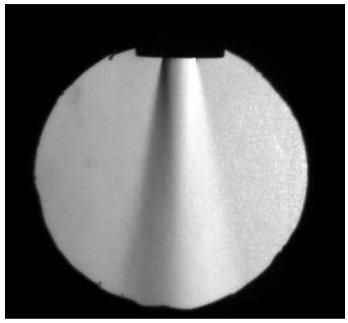

Figure 6. Subcritical injection at Tr=1.00, Pr=0.11, m_{ratio}=0.0, S_m=0.0.

In previous works using schlieren to observe the features of supercritical jets [13,14], the issue of exceeding the schlieren measuring range was less noticeable as the CO_2 concentration was rapidly reduced by mixing with air. However, Zeaton [14] and Doungthip [13] both observed refractivity gradients exceeding the measuring range for jets with no-swirl or very low levels of swirl, where the jet mixing rate was lower. In the present work, this phenomenon was even observed in the S_m = 1.77 images, indicating a solid cone of supercritical CO_2 exiting the injector, as seen in Figure 7.

Downstream of the injector exit, the jet develops into a hollow cone, where only its periphery is visible. The development of the hollow cone indicates that VB is occuring, as the CO_2 vortex breaks, and air is allowed to recirculate into the vortex interior.

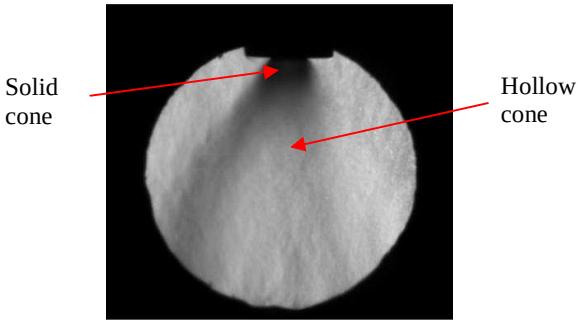

Figure 7. Supercritical injection at Tr=1.05, Pr=1.05, m_{ratio}=1.0, S_m=1.77.

Despite exceeding the refractive index gradient measuring range, valuable results were extracted from the schlieren images. The jet spreading half angles were measured directly from the images as

$$\frac{\theta}{2} = \arctan\left(\frac{width}{length}\right) \quad (3)$$

and the full angles are reported here.

Zeaton [14] found the spreading angles of supercritical jets to depend strongly on swirl number, more so than on other variables such as density ratio. The general trend of the current data can be noted by comparing the images corresponding to the different mass ratios, at otherwise similar operating conditions (Figures 5, 7 and 8). The jet spreading angles as a function of swirl number and density ratio are shown in Figure 9. Included for comparison are the final jet spreading angles reported by Zeaton [14]. An important difference between the two data sets is that Zeaton [14] defined his swirl number according to geometry (S_g), and it is here defined according to momentum.

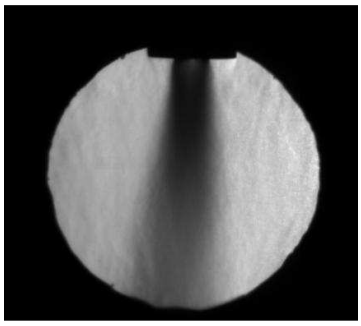

Figure 8. Supercritical injection at Tr=1.02, Pr=1.05, m_{ratio} = 0.150, S_m= 0.130.

Regardless, the present results show reasonable agreement in that the spreading angle increases with swirl number, more so than with increasing density ratio, except for the case with S_m=0.0 and S_g=0.0, where the measured spreading angles (8.0, 8.4 and 7.2°) show better agreement with turbulent jet correlations [18], which predict an angle of 10°.

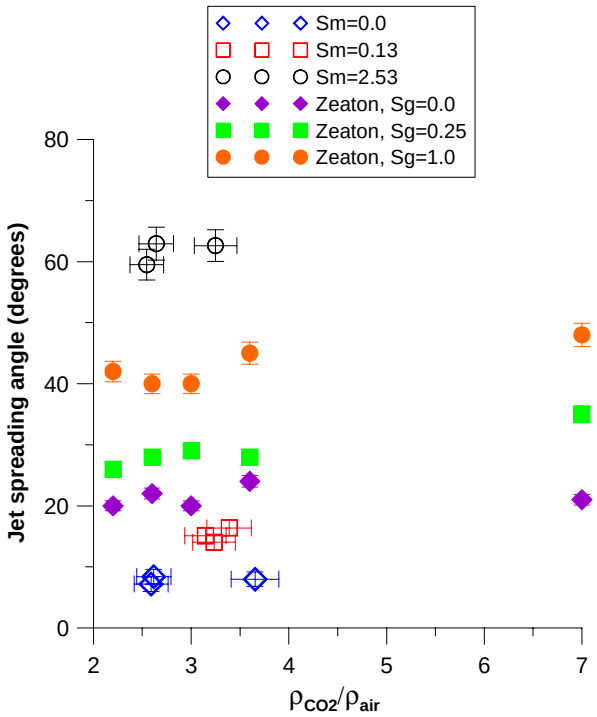

Figure 9. Effect of swirl number and density ratio on jet spreading angle.

CONCLUSIONS

A computational model of VB was developed to aid in the design and operation of an axial-plus-tangential supercritical fuel injector. The model produced a curve of swirl number as a function of input mass ratio.

Schlieren images were captured, and cone angles were measured for supercritical fuel injection and swirl numbers of 0.0, 0.14 and 2.5. The results were analyzed to determine how cone angle scaled with swirl number and density ratio. The following conclusions were drawn:

1. Spreading angle behaved as expected when swirl number and density ratio were changed: the angle increased with swirl number. Good agreement was also seen between the no-swirl case and the turbulent jet literature.
2. The change from a solid- to hollow-cone structure in the high swirl case indicates the occurrence of VB. This occurrence will be the subject of future investigations utilizing laser Doppler anemometry to accurately measure the velocity fields.

REFERENCES

[1] D. Peckham and S. Atkinson, Preliminary Results of Low Speed Wind Tunnel Tests on a Gothic Wing of Aspect Ratio 1.0, Aeronautical Research Council Report CP 508.

[2] M. Escudier, Vortex Breakdown: Observations and Explanations, *Progress in Aerospace Sciences*, vol. 25, no.2, pp. 189-229, 1988.

[3] J. Delery, Aspects of Vortex Breakdown, *Progress in Aerospace Sciences*, vol. 30, no.1, pp. 1-59, 1994.
[4] O. Lucca-Negro and T. O'Doherty, Vortex Breakdown: A Review, *Progress in Energy and Combustion Science*, vol. 27, no. 4, pp. 431-481, 2001.
[5] J. Beer and N. Chigier, Combustion Aerodynamics, John Wiley and Sons, New York, 1972.
[6] P. Billand, J. Chomaz and P. Huerre, Experimental study of vortex breakdown in swirling jets, *Journal of Fluid Mechanics*, vol. 376, pp. 183-219, 1998.
[7] A. Garg and S. Leibovich, Spectral characteristics of vortex breakdown flowfields, *Physics of Fluids*, vol. 22, no.11, pp. 2053-2064, 1979.
[8] T. Sarpkaya, On Stationary and Travelling Vortex Breakdown, *Journal of Fluid Mechanics*, vol. 45, no. 3, pp. 545-559, 1971.
[9] K. Midgley, A. Spencer, and J. McGuirk, Unsteady Flow Structures in Radial Swirler Fed Fuel Injectors, *Journal of Engineering for Gas Turbines and Power-Transactions of the ASME*, vol. 127, no. 4, pp. 755-764, 2005.
[10] G. Li and E. Gutmark, Flow Field Measurements of a Triple-Annular Spray Combustor, *AIAA Paper No. 2002-4010*, 2002.
[11] G. Li and E. Gutmark, Geometry Effects on the Flow Field and the Spectral Characteristics of a Triple Annular Swirler, *ASME GT-2003-38799*, 2003.
[12] T. Edwards, Cracking and Deposition Behavior of Supercritical Hydrocarbon Aviation Fuels, *Combustion Science and Technology*, vol. 178, no. 1-3, pp. 307-334, 2006.
[13] T. Doungthip, J. Ervin, T. Williams and J. Bento, Studies of Injection of Jet Fuel at Supercritical Conditions, *Industrial and Engineering Chemistry Research*, vol. 41, pp. 5856-5866, 2002.
[14] G. Zeaton, M.S. thesis, Purdue University, West Lafayette, Indiana, 2004.
[15] N. Chigier and A. Chervinsky, Experimental Investigations of Swirling Vortex Motions in Jets, *Journal of Applied Mechanics*, vol. 34, no. 2, pp. 443-451.
[16] S. Pope, Turbulent Flows, Cambridge University Press, New York, 2000.
[17] G. Settles, Schlieren and Shadowgraph Techniques, Spring, New York, 2001.
[18] S. Turns, An Introduction to Combustion: Concepts and Applications, 2nd ed., McGraw Hill, New York, 2000.